NANO LETTERS

2009
Vol. 9, No. 6
2372-2377

Fabry-Pérot Resonances in One-Dimensional Plasmonic Nanostructures

Jens Dorfmüller,*,† Ralf Vogelgesang,*,† R. Thomas Weitz,† Carsten Rockstuhl,‡ Christoph Etrich,¶ Thomas Pertsch,¶ Falk Lederer,‡ and Klaus Kern†,§

Max-Planck-Institut für Festkörperforschung, Heisenbergstr. 1, 70569 Stuttgart, Germany, Institut für Festkörpertheorie and -optik, Friedrich-Schiller-Universität Jena, Max-Wien-Platz 1, 07743 Jena, Germany, Institut für angewandte Physik, Friedrich-Schiller-Universität Jena, Max-Wien-Platz 1, 07743 Jena, Germany, and Institut de Physique des Nanostructures, École Polytechnique Fédérale de Lausanne, 1015 Lausanne, Switzerland

Received March 20, 2009; Revised Manuscript Received May 11, 2009

ABSTRACT

We study the near-field optical behavior of Fabry-Pérot resonances in thin metal nanowires, also referred to as quasi one-dimensional plasmonic nanoantennas. From eigenmodes well beyond quadrupolar order we extract both, propagation constant and reflection phase of the guided surface plasmon polariton with superb accuracy. The combined symmetry breaking effects of oblique illumination and retardation allow the excitation of dipole forbidden, even order resonances. All measurements are supported by rigorous simulations of the experimental situation.

Introduction. In recent years surface plasmon polaritons (SPPs)—either propagating or localized at metal−dielectric interfaces—have attracted renewed interest. On the one hand, advances in nanotechnology made the fabrication of resonant plasmonic structures feasible even for visible wavelengths. On the other hand, a growing variety of near-field optical characterization techniques are coming of age. Resonant plasmonic structures for applications at terahertz to visible wavelengths can now be studied by means well beyond conventional far-field scattering spectroscopy of particle ensembles.[1,2] Two-photon luminescence (TPL) provides spectroscopic access to single wire structures,[3,4] and several techniques break the spatial diffraction limit of resolution, including electron energy loss spectroscopy (EELS),[5−7] photoemission electron microscopy (PEEM),[8−10] and scanning near-field optical microscopy (SNOM).[11−15]

At the same time, exciting ideas for applications of plasmonic resonances spring up with unabated frequency: as novel ultrasensitive sensors,[16−18] as heat concentrating agents in cancer treatment,[19] as building blocks of metamaterials,[20] or as active elements in all-optical signal processing.[21−23] To further advance the rational design of resonant plasmonic structures, precise knowledge of the relation between design parameters and resonance conditions is crucial. Specifically for guided plasmonic waves, the precise measurement of *both* the propagation and reflection parameters allows optimal impedance matching to transmission lines,[24] single molecules,[25] or even quantum dots[26] with possible application in quantum computing. A better understanding of nanoscopic resonance mechanisms will also advance the fields of ultrafast nano-optics, e.g., by improving the design of new structures for coherent control.[27,28]

Here, we measure the wavelength and reflection phase of plasmons in thin metal wires of finite length with sufficient accuracy to compare against theoretical models.[29−32] Such quasi-one-dimensional metallic structures are frequently also referred to as optical antennas in the literature.[29,31,32]In the following, to prevent confusion, we adopt the term "metal nanowire" or short "wire". This prototypical system can be described as Fabry-Pérot resonators for guided quasi-one-dimensional plasmons. With an improved variant of apertureless SNOM (aSNOM), we obtain images of amplitude and phase of local electric field components. As in combinatorial material science,[33] a limited number of images allow us to study a large number of isolated structures under virtually identical conditions, facilitating direct and quantitative analysis of the full system. From the lowest order resonances we obtain experimental values for the propagation

* Corresponding authors, J.Dorfmueller@fkf.mpg.de and R.Vogelgesang@fkf.mpg.de.

† Max-Planck-Institut für Festkörperforschung.

‡ Institut für Festkörpertheorie and -optik, Friedrich-Schiller-Universität Jena.

¶ Institut für angewandte Physik, Friedrich-Schiller-Universität Jena.

§ Institut de Physique des Nanostructures, École Polytechnique Fédérale de Lausanne.

10.1021/nl900900r CCC: $40.75
Published on Web 05/27/2009

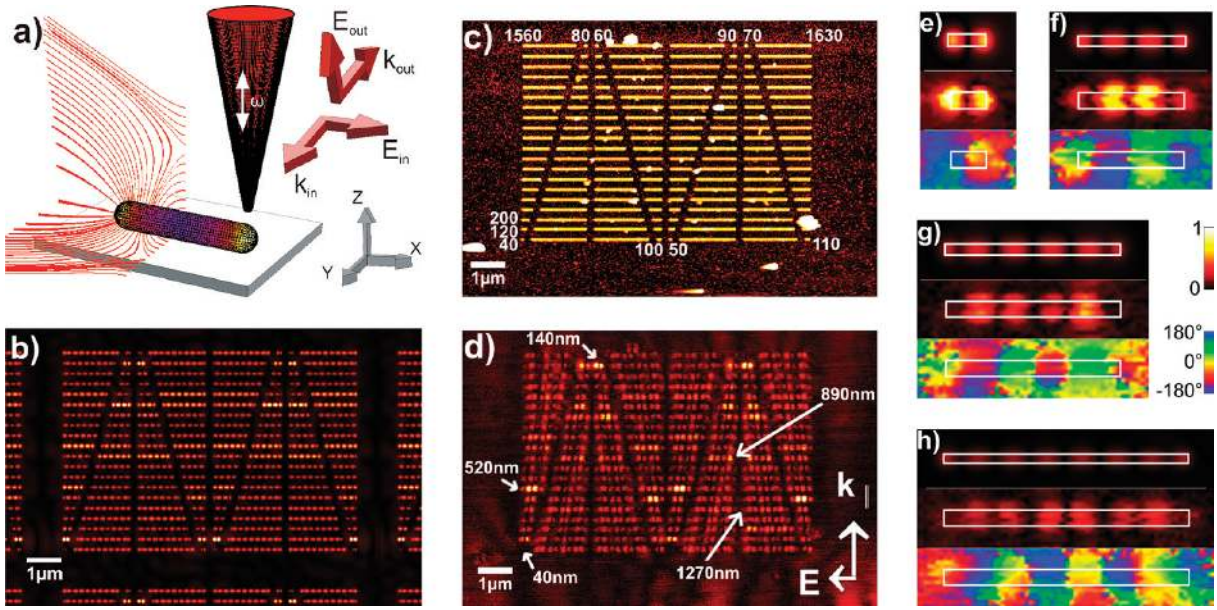

Figure 1. (a) Scheme of the setup. Weakly focused s-polarized radiation excites nanowires largely unperturbed by the probing tip. A typical response field is indicated by the electric field strength distribution on the wire surface and a snapshot of selected field lines. Backscattered light is modulated by the tip vibration (frequency ω) and polarization-analyzed along the tip axis. (b) Simulated magnitude of the z-component of the electric field 24 nm above the structure shown in (c). (c) Topography of the metallic nanowires. The wires of different length are arranged in a compact manner, though sufficiently separated to reasonably assume they are noninteracting. (d) Simultaneously obtained, baseline-corrected near-field optical amplitude image for an excitation wavelength of $\lambda = 942$ nm. (e−h) Compound images of simulated magnitude (top), measured magnitude (middle), and phase (bottom) for the 140, 520, 890, and 1270 nm long wires, respectively, which represent the odd order resonances. White rectangles indicate the contours of the wires as taken from the nominal and measured geometry.

as well as the reflection[29−32] of plasmons. We nicely confirm that the symmetry-forbidden even-order modes are accessible with off-axis excitation. Quantitatively, our results are in good agreement with simulations. However, we find small, systematic deviations attributed to device imperfections and/or overly idealized modeling, specifically concerning the intriguing behavior of the wire terminations.

Methods and Materials. We use aSNOM to analyze the near-field distribution around metallic nanostructures. The e-beam-lithographically written nanostructures are located on a silicon oxide substrate that is illuminated under an angle of about 71° relative to the substrate normal. A commercial atomic force microscope (AFM) tip in noncontact mode scatters the local electromagnetic near-fields around the structures back toward the far-field detector. To discriminate the near-field content of the backscattered light, we analyze the recorded signal with a lock-in amplifier at higher harmonic frequencies of the tip vibration frequency. By raster scanning the sample underneath the tip, we obtain near-field information across large areas with the typical aSNOM resolution of about 10 nm.[34]

To suppress perturbation of the near-field at the nanostructures by the tip to the largest possible extent, we rely on a cross-polarization scheme where the illuminating and the scattered field components are orthogonally polarized.[35] For the excitation of the sample we use s-polarized light. This polarization hardly excites the tip at all.[36] In contrast, the structures on the sample may respond with strong plasmonic resonances. The tip efficiently picks up the vertical field components of these resonances and scatters them back into the far-field as mainly p-polarized light. As we have shown earlier (ref 35), recorded images represent maps of the normal component of the undisturbed eigenmode near-fields.

The experimental situation at the sample is illustrated in Figure 1a. An s-polarized beam from a tunable continuous wave light source (Ti:Sa, Coherent 899) tuned to 942 nm wavelength excites the sample near grazing incidence (≈19° off the sample surface). It is focused onto a commercial noncontact AFM tip (Nanosensors AdvancedTEC NC), oscillating around a mean distance of about 20 nm above the surface. The backscattered light is amplified with an interferometric detection scheme which provides access to both the optical amplitude and phase.[34,37]

The gold nanostructures are prepared on heavily doped silicon wafers coated with a 100 nm silicon oxide layer. Smooth, 25 nm high Au structures are prepared by standard electron beam lithography, thermal metal deposition, and lift-off using a 0.3−0.5 nm Ti adhesive layer, whose influence on optical properties can be neglected. We investigate 40 nm wide wires with a length distribution from 40 to 1630 nm in steps of 10 nm. In one part of the study, wires are arranged in several interlaced columns as shown in Figure 1c with a surface-to-surface spacing of 260 nm. Scanning electron microscopy (SEM) analysis confirms that actual sample parameters agree with the nominal values to within the SEM resolution. To study excitation conditions for the lowest even order eigenmode in detail, we use an array of 40 nm wide wires that has been randomized both in length

(280, 300,..., 360 nm) and azimuthal angle (−90°, −75°,..., 90°) (see Figure 3a).

To compare with theoretical predictions, we perform extensive FDTD simulations.[38] The spatial domain is discretized with a resolution of 8 nm. For the refractive index we use values reported in the literature:[39] $n_{Au} = 0.198 + 6.046i$, $n_{SiO_2} = 1.536$, and $n_{Si} = 3.638$ at $\lambda = 942$ nm. The semi-infinite half-space above the substrate is assumed to be air. The sample shown in Figure 1c is entirely discretized as one supercell and arranged periodically in lateral directions to make use of periodic boundary conditions with periods of 9.696 and 6.896 μm—large enough to exclude interactions with neighboring supercells. The wires shown in Figure 3a are simulated individually with a square periodicity of 1 μm. In the normal direction we assume perfectly matched layers. The structures are illuminated with s-polarized plane waves at an incidence angle of 71° with respect to the surface normal, reproducing exactly the experimental conditions.

The simulations do not include any probing tip. The measured signal is taken to be the normal component of the local electromagnetic field in a plane 24 nm above the structure. On the basis of our cross-polarization scheme,[35] this assumption is justified a posteriori by the excellent agreement between experimental and numerical data.

Results and Discussion. Figure 1d displays the near-field image of the sample shown in Figure 1c recorded with excitation polarization parallel to the wire axis. For presentation, the image has been corrected with a line-by-line removal of a small complex-valued offset, attributed to remnants of parasitic background scattering. This does not affect the following analysis. Evidently, the signal strength varies strongly from wire to wire. The shortest, 40 nm long wire exhibits a very weak signal while the 140 nm long wire gives the strongest signal. Its modal field distribution (see Figure 1e) is characterized by two amplitude lobes and a single nodal line in between. This clear indication of a dipolar mode is also confirmed by the optical phase image which shows a difference in phase between the two lobes of about 180°. Longer wires show higher order resonances, enumerated by the number of node-lines crossed along the length of the wire. Thus, the third-order resonance is observed for a wire length of ≈520 nm (Figure 1f) and the fifth for ≈890 nm (Figure 1g). In Figure 1b we show the z-component of the **E**-field 24 nm above the structure, as extracted from an FDTD simulation of the full structure. Comparing experiment and simulation shows a good agreement in the distribution of (near-) resonant wires as well as the modal structure of the individual wires.

The general interpretation of these observations is plasmonic standing waves patterns.[40] That is, inside the metal volume the charge density exhibits localized lobes of alternating sign along the wire length which oscillate in time. Associated electromagnetic fields are both effect and driving force of these fluctuations. As depicted in Figure 1a for the first-order mode, outside the metal/dielectric interface the cross-polarized aSNOM probes the electric field component along the tip shaft. Only odd order modes are observed to show strong local fields in Figure 1d. The even order modes, which are mirror symmetric about the y-z-plane, are fundamentally mismatched to the antisymmetric excitation.

For the symmetry-allowed odd modes, a more detailed comparison of the measured versus simulated signal reveals small differences for individual wires, particularly for higher order resonances (Figure 1e−h). Generally, the measured local field strength at the ends is found to be considerably lower than at the central lobes and the inner lobes exhibit a tendency to pair up. At present, simulation does not lend a simple explanation, showing hardly any accents on different lobes of a given resonance.

Examining the system of wires as a whole, we identify the resonance lengths by extracting the maximum amplitude per wire. Figure 2a shows a plot of these maxima against wire length. Geometric resonances up to seventh order are clearly observed as peaks. With increasing resonance order, the peak amplitude drops and the width broadens. By fitting these peaks with Lorentzians, we obtain the resonant lengths for the different orders. The first-order resonance can be observed at a wire length of 143 nm. From the simulation shown in Figure 1b we obtain an equivalent curve. As a first finding, the resonances appear slightly shifted toward smaller wire lengths compared to experiment. Figure 2b shows the resonance wire length as a function of resonance order, which is nicely approximated by a linear fit for both experimental and simulated data

$$L_{exp}(n) = -(43.7 \pm 1.4)\ \text{nm} + n\,(186.4 \pm 0.9)\ \text{nm} \quad (1)$$

$$L_{sim}(n) = -(47.7 \pm 0.8)\ \text{nm} + n\,(180.7 \pm 0.6)\ \text{nm} \quad (2)$$

where n is the resonance order. In an intuitive and clear interpretation of these observations the nanowires may be regarded as one-dimensional Fabry-Pérot resonators. Guided SPPs travel along the wire length L with a propagation constant γ and suffer a phase jump $\delta\phi$ upon reflection at each end. For the nth order resonant wire length the total round trip phase accumulation equals n times 2π

$$2\gamma L(n) + 2\delta\phi = 2\pi n \quad (3)$$

Our measured spacing between subsequent resonant, odd-order wire lengths thus provides an unambiguous unit of one plasmon wavelength, $\lambda_p = 2\pi/\gamma = 372.8$ nm. It compares very well to a finite element method mode solver derived value of 371 nm for the wavelength of an infinite plasmonic waveguide of identical cross section.

The phase change $\delta\phi = 42.2°$ at the wire ends, though, is somewhat ambiguous. Viewing the nanowires as optical nanoantennas[29] suggests an alternative way to interpret this quantity as an apparent length increase $\delta L = \delta\phi/\gamma$. Either description is independent of resonance order n and represents a reactance-related property specific to the wire-terminating structure. However, differing conventions are possible of what constitutes "the" nanowire length for rounded or tapered ends, etc., depending on whether the cap is counted as part of the wire or not. As we regard our cross-sectional end facets as nearly flat, we have a unique length

definition for wire antennas. In this light, we judiciously note that the 40 nm width and 25 nm height of our rectangular, substrate-supported, flat-end wires compares well with the 43.7 nm diameter that would be derived following ref 29 from eq 1 for circular, in vacuo, hemispherically capped wires. The small systematic deviations of the simulated values (eq 2) from our experimental data (eq 1) may have several reasons, such as the imprecise knowledge of n_{Au} of thermally deposited gold or the idealized simulated wire geometry including abruptly sharp edges and corners.

Beyond characterizing plasmonic wires using the symmetry allowed odd order resonances our aSNOM approach also allows us to study the resonances with an even number of nodes. In our experiment, this symmetry constraint is easily lifted by changing the azimuthal angle of the sample relative to the excitation. Thanks to retardation, for skew incidence, the **E**-field varies over the length of the wire and its projection onto the wire axis contains a mirror symmetric part, which thus enables the excitation of even modes. By analyzing an image recorded with the sample rotated by 20° (not shown), we obtain the resonance curve shown in Figure 2c. Most prominently, besides the peaks previously observed (red lines), additional resonance peaks (blue lines) appear at the even order resonance lengths all with nearly the same amplitude. Apparently, the dipole coupling strength of odd order modes to the excitation rapidly diminishes for longer wires, whereas the retardation-enabled coupling of even modes remains equally strong.

Fitting the peaks in the same manner as before leads to

$$L_{exp}(n) = -(31.7 \pm 0.9)\ \text{nm} + n\,(180.9 \pm 0.6)\ \text{nm} \quad (4)$$

$$L_{sim}(n) = -(47.6 \pm 0.8)\ \text{nm} + n\,(180.2 \pm 0.6)\ \text{nm} \quad (5)$$

The fitting parameters derived from simulation hardly vary between eq 2 and 5, the corresponding experimental values change significantly from eq 1 to 4. We attribute the significant difference in the offset value between eqs 4 and 5 to imperfect knowledge of the precise geometrical features of the fabricated wire ends, which are simulated as perfectly flat. While these findings will be subject of further, more detailed studies, in the next two paragraphs we concentrate on the angle and length dependence of the lowest even order resonance, which has received only little attention in the literature.[10,30] We analyze an array of wires with lengths distributed around the second-order resonance and arranged with varying azimuthal orientations. Figure 3b shows this mode with three lobes and two nodes. We note that the "front" lobe (as seen from the incident radiation's point of view) appears characteristically weaker than the middle and back lobe. Analyzing all wires in the same manner as before results in the two-dimensional contour plot shown in Figure 3c. From a set of individual simulations of each wire we extract the corresponding contour plot shown in Figure 3d.

On the whole, both contour plots agree. The resonance wire lengths appear at ≈330 nm in experiment and ≈310 nm in simulation, consistent with eqs 1 and 2, respectively. At the resonance wire length, both plots show maxima at about ±45° as clear indication of an excitation of the even order plasmonic mode. Symmetry suppression explains the minima at 0 and at ±90°. The directional dependence of

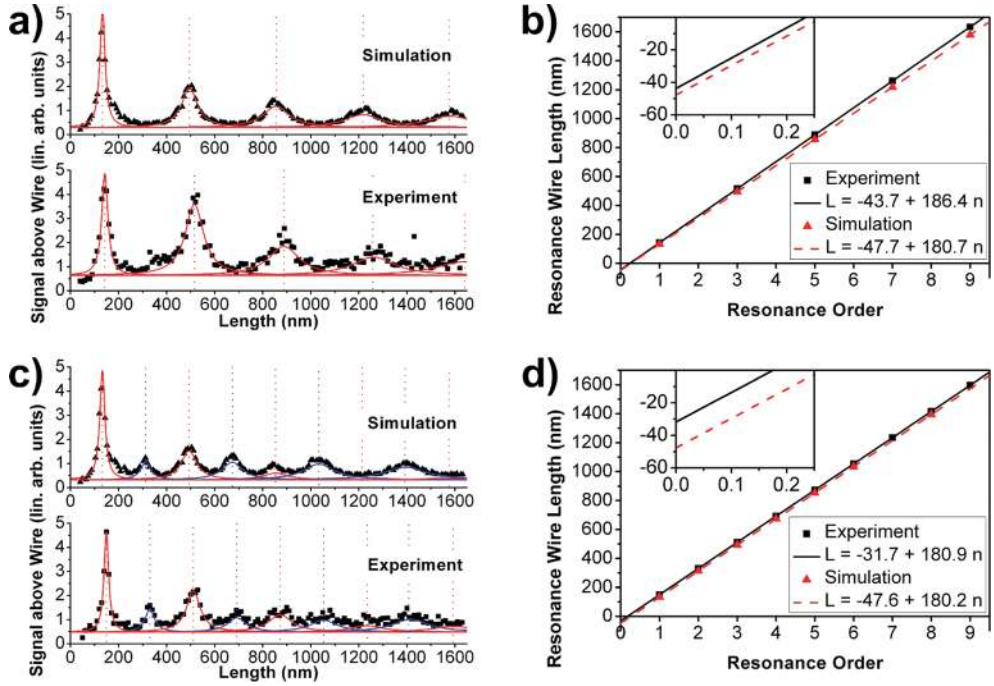

Figure 2. (a) Resonance curves obtained by plotting the maximum signal per wire versus the wire length. The experimental and simulation data have been extracted from Figure 1. The solid lines show Lorentzians fitted to the data. (b) Plot of the Lorentzians' peak positions versus the resonance order. The lines are a least-squares fit to the data. The inset is a zoom where the fitted straight lines cross the *y* axis. (c) Resonance curves when the sample is rotated by ≈20°. (d) Resonance length versus resonance plot of the rotated sample.

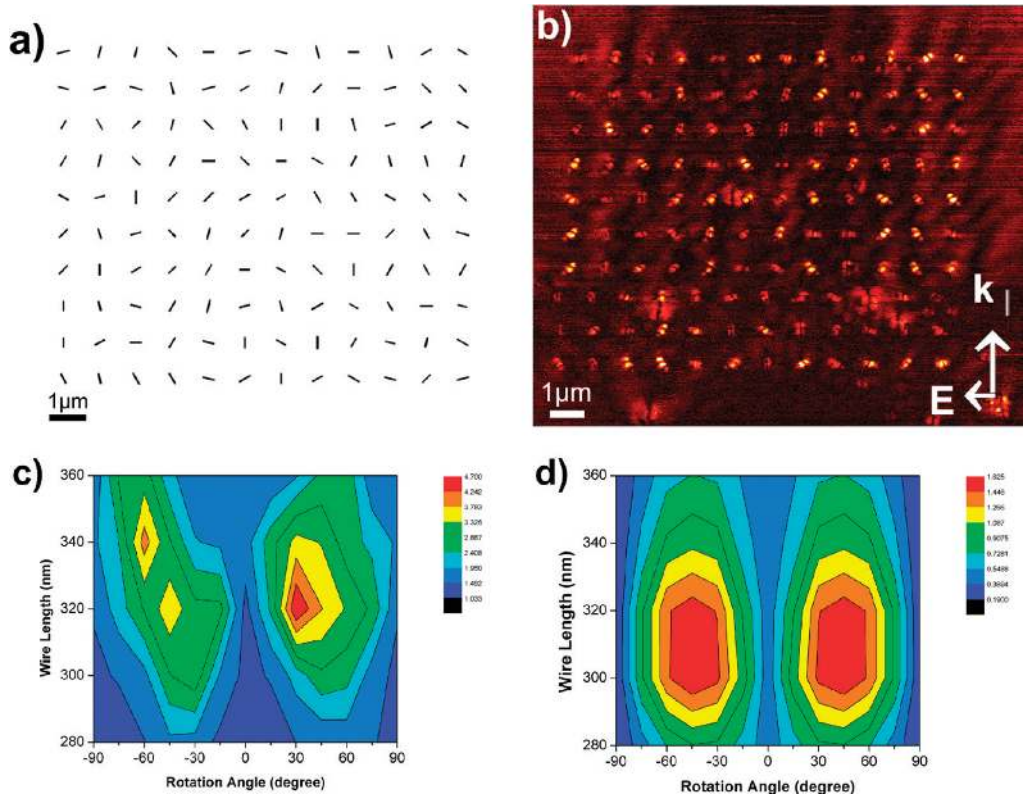

Figure 3. (a) Design of the sample to study the second-order resonance. The length and the rotation angle of the wires are varied from 280 to 360 nm and from −90 to 90°. (b) Baseline-corrected optical near-field amplitude of the respective sample at an illumination wavelength of $\lambda = 942$ nm. (c) Detailed analysis of the second-order resonance: The maximum signal obtained from each wire is plotted in a 2D angle—wire length—contour plot. The minimum between the two peaks shows that the second-order resonance is symmetry forbidden at an angle of 0°. (d) Similar plot obtained from FDTD simulations. The wires of the sample have been simulated individually.

excitation—as studied here for the second-order mode—could be of use in future applications, for example to tune the response of individual structures by the directionality of the external source or to allow efficient multiwavelength optical excitation of nanowires by multidirectional illumination.

Conclusion and Outlook. In summary, we characterize the fundamental system of thin metal nanowires from their lowest order Fabry-Pérot resonances. This demonstrates the considerable value of cross-polarized aSNOM for the quantitative investigation of resonant plasmonic nanostructures in general. We note that our measurements reveal a slight dependence of the Fabry-Pérot modes on excitation *orientation*. This might suggest novel routes to fine-tune resonant nanoplasmonic responses, especially concerning phase control and directional selectivity.

From a more fundamental point of view, the behavior of wire termination leaves a number of open questions. The observed suppressed field amplitudes at the wire ends may be an indication of locally enhanced damping due to pronounced electron scattering at the end facets. The specific phase jump upon reflection at the wire ends (or apparent length increase) is reminiscent of the phase shifts (or apparent penetration depths) associated with total internal reflection phenomena, such as the Goos-Hänchen effect. For planar waves at two-dimensional interfaces, matching single modes on either side provides a complete analytical description. However, the reflection of surface or wire plasmon polaritons at one-dimensional edges or wire terminations, respectively, needs more sophisticated modeling,[31,42] matching continua of modes on each side. We anticipate that studies like the present one will contribute significantly to the microscopic understanding of low-dimensional reflection and impedance mismatch phenomena.

References

(1) Krenn, J. R.; Schider, G.; Rechberger, W.; Lamprecht, B.; Leitner, A.; Aussenegg, F.; Weeber, J.-C. *Appl. Phys. Lett.* **2000**, *77*, 3379–3381.
(2) Schider, G.; Krenn, J. R.; Hohenau, A.; Ditlbacher, H.; Leitner, A.; Aussenegg, F.; Schaich, W.; Puscasu, I.; Monacelli, B.; Boreman, G. *Phys. Rev. B* **2003**, *68*, 155427.
(3) Mühlschlegel, P.; Eisler, H.-J.; Martin, O. J. F.; Hecht, B.; Pohl, D. W. *Science* **2005**, *308*, 1607–1609.
(4) Ghenuche, P.; Cherukulappurath, S.; Taminiau, T. H.; van Hulst, N. F.; Quidant, R. *Phys. Rev. Lett.* **2008**, *101*, 116805.
(5) Nelayah, J.; Kociak, M.; Stephan, O.; García de Abajo, F. J.; Tence, M.; Henrard, L.; Taverna, D.; Pastoriza-Santos, I.; Liz-Marzan, L. M.; Colliex, C. *Nat. Phys.* **2007**, *3*, 348–353.
(6) Bosman, M.; Keast, V. J.; Watanabe, M.; Maaroof, A. I.; Cortie, M. B. *Nanotechnology* **2007**, *18*, 165505.
(7) García de Abajo, F. J.; Kociak, M. *Phys. Rev. Lett.* **2008**, *100*, 106804.
(8) Schmidt, O.; Bauer, M.; Wiemann, C.; Porath, R.; Scharte, M.; Andreyev, O.; Schonhense, G.; Aeschlimann, M. *Appl. Phys. B: Lasers Opt.* **2002**, *74*, 223–227.
(9) Bayer, D.; Wiemann, C.; Gaier, O.; Bauer, M.; Aeschlimann, M. *J. Nanomater.* **2008**, *2008*, 249514.
(10) Douillard, L.; Charra, F.; Korczak, Z.; Bachelot, R.; Kostcheev, S.; Lerondel, G.; Adam, P.-M.; Royer, P. *Nano Lett.* **2008**, *8*, 935–940.

(11) Hillenbrand, R.; Keilmann, F.; Hanarp, P.; Sutherland, D. S.; Aizpurua, J. *Appl. Phys. Lett.* **2003**, *83*, 368–370.
(12) Imura, K.; Nagahara, T.; Okamoto, H. *J. Phys. Chem. B* **2004**, *108*, 16344–16347.
(13) Imura, K.; Nagahara, T.; Okamoto, H. *J. Chem. Phys.* **2005**, *122*, 154701.
(14) Lee, K. G.; Kihm, H. W.; Kihm, J. E.; Choi, W. J.; Kim, H.; Ropers, C.; Park, D. J.; Yoon, Y. C.; Choi, S. B.; Woo, D. H.; Kim, J.; Lee, B.; Park, Q.-H.; Lienau, C.; Kim, D. S. *Nat. Photonics* **2007**, *1*, 53–56.
(15) Rang, M.; Jones, A. C.; Zhou, F.; Li, Z.-Y.; Wiley, B. J.; Xia, Y.; Raschke, M. B. *Nano Lett.* **2008**, *8*, 3357–3363.
(16) Aizpurua, J.; Hanarp, P.; Sutherland, D. S.; Kall, M.; Bryant, G. W.; García de Abajo, F. J. *Phys. Rev. Lett.* **2003**, *90*, 057401.
(17) Hao, F.; Nehl, C. L.; Hafner, J. H.; Nordlander, P. *Nano Lett.* **2007**, *7*, 729–732.
(18) Hao, F.; Sonnefraud, Y.; Dorpe, P. V.; Maier, S. A.; Halas, N. J.; Nordlander, P. *Nano Lett.* **2008**, *8*, 3983–3988.
(19) Hirsch, L.; Stafford, R.; Bankson, J.; Sershen, S.; Rivera, B.; Price, R.; Hazle, J.; Halas, N. J.; West, J. L. *Proc. Natl. Acad. Sci. U.S.A.* **2003**, *100*, 13549–13554.
(20) Zentgraf, T.; Dorfmüller, J.; Rockstuhl, C.; Etrich, C.; Vogelgesang, R.; Kern, K.; Pertsch, T.; Lederer, F.; Giessen, H. *Opt. Lett.* **2008**, *33*, 848–850.
(21) Barnes, W. L.; Dereux, A.; Ebbesen, T. W. *Nature* **2003**, *424*, 824–830.
(22) Zia, R.; Schuller, J. A.; Chandran, A.; Brongersma, M. L. *Mater. Today* **2006**, *9*, 20–27.
(23) Wurtz, G. A.; Hendren, W.; Pollard, R.; Atkinson, R.; Guyader, L. L.; Kirilyuk, A.; Rasing, T.; Smolyaninov, I. I.; Zayats, A. V. *New J. Phys.* **2008**, *10*, 105012.
(24) Huang, J.-S.; Feichtner, T.; Biagioni, P.; Hecht, B. *Nano Lett.* **2009**, *9*, 1897–1902.
(25) Greffet, J.-J. *Science* **2005**, *308*, 1561–1563.
(26) Akimov, A. V.; Mukherjee, A.; Yu, C. L.; Chang, D. E.; Zibrov, A. S.; Hemmer, P. R.; Park, H.; Lukin, M. D. *Nature* **2007**, *450*, 402–406.
(27) Stockman, M.; Faleev, S.; Bergman, D. *Phys. Rev. Lett.* **2002**, *88*, 067402.
(28) Aeschlimann, M.; Bauer, M.; Bayer, D.; Brixner, T.; García de Abajo, F. J.; Pfeiffer, W.; Rohmer, M.; Spindler, C.; Steeb, F. *Nature* **2007**, *446*, 301–304.
(29) Novotny, L. *Phys. Rev. Lett.* **2007**, *98*, 266802.
(30) Encina, E. R.; Coronado, E. A. *J. Phys. Chem. C* **2008**, *112*, 9586–9594.
(31) Barnard, E. S.; White, J. S.; Chandran, A.; Brongersma, M. L. *Opt. Express* **2008**, *16*, 16529–16537.
(32) Bryant, G. W.; García de Abajo, F. J.; Aizpurua, J. *Nano Lett.* **2008**, *8*, 631–636.
(33) Hanak, J. J. *J. Mater. Sci.* **1970**, *5*, 964–971.
(34) Bek, A.; Vogelgesang, R.; Kern, K. *Rev. Sci. Instrum.* **2006**, *77*, 043703.
(35) Esteban, R.; Vogelgesang, R.; Dorfmüller, J.; Dmitriev, A.; Rockstuhl, C.; Etrich, C.; Kern, K. *Nano Lett.* **2008**, *8*, 3155–3159.
(36) Novotny, L.; Bian, R.; Xie, X. *Phys. Rev. Lett.* **1997**, *79*, 645–648.
(37) Ocelic, N.; Huber, A.; Hillenbrand, R. *Appl. Phys. Lett.* **2006**, *89*, 101124.
(38) Taflove, A.; Hagness, S. C. *Computational Electrodynamics: The Finite-Difference Time-Domain Method*, 3rd ed.; Artech House: Boston, 2005.
(39) Johnson, P. B.; Christy, R. W. *Phys. Rev. B* **1972**, *6*, 4370–4379.
(40) Søndergaard, T.; Beermann, J.; Boltasseva, A.; Bozhevolnyi, S. I. *Phys. Rev. B* **2008**, *77*, 115420.
(41) Goos, F.; Hänchen, H. *Ann. Phys. (Weinheim, Ger.)* **1947**, *1*, 333–346.
(42) Gordon, R. *Phys. Rev. B* **2006**, *74*, 153417.

NL900900R